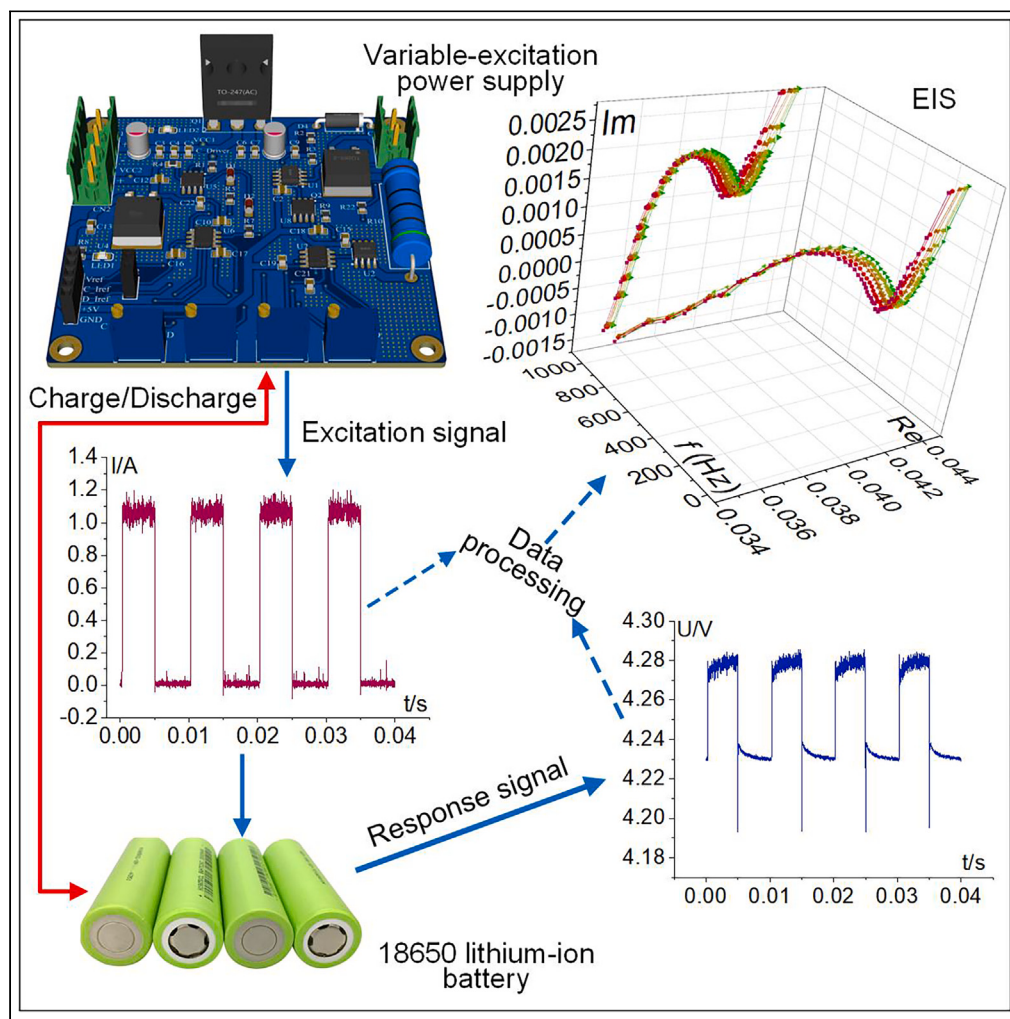


## Article

## Fast electrochemical impedance spectroscopy of lithium-ion batteries based on the large square wave excitation signal



Lujun Wang, Ziang Song, Lijun Zhu, Jiuchun Jiang

jcjiang@hbut.edu.cn

**Highlights**

Introducing an EIS testing method based on the large square wave excitation signal

Design of variable-excitation power supply for EIS testing

Estimation of SOH of lithium-ion batteries



## Article

# Fast electrochemical impedance spectroscopy of lithium-ion batteries based on the large square wave excitation signal

Lujun Wang,<sup>1,2</sup> Ziang Song,<sup>1,2</sup> Lijun Zhu,<sup>1</sup> and Jiuchun Jiang<sup>1,3,\*</sup>

## SUMMARY

**Electrochemical impedance spectroscopy (EIS) is a technique for electrochemical characterization that is sensitive to the battery state and can uncover multidimensional electrochemical evolution information within the battery. Lithium-ion batteries usually need to be used in conjunction with power conversion circuits, while conventional EIS testing is conducted offline and is time-consuming, which cannot effectively monitor the battery characteristics during use. To match the characteristics of the square wave signal during power switching, a rapid EIS measurement method for lithium-ion batteries based on the large square wave excitation signal is proposed in this paper, and develops a testing device with a response time of microseconds. The proposed method and device are applied to estimate the state of health (SOH) of the battery. In conclusion, we proposed method enhances the capabilities of EIS testing technology and has a good application prospect in real-time online impedance monitoring.**

## INTRODUCTION

With its advantages of large capacity, high working voltage, and long cycle life, lithium-ion battery stands out from many electrochemical energy storage devices and is widely used. During long-term use, lithium-ion batteries' electrochemical performance and safety status will degrade, which may lead to serious consequences such as thermal runaway. Therefore, conducting rapid and accurate condition assessments and safety monitoring of lithium-ion batteries is important.<sup>1–3</sup>

Electrochemical impedance spectroscopy (EIS) is an electrochemical characterization technique that directly measures the impedance characteristics of batteries and further estimates the internal state of the battery from the impedance characteristics.<sup>4,5</sup> The conventional EIS measurement employs a single-frequency sine wave excitation signal and the testing process is performed offline with a relatively long testing time. Fast EIS testing employs non-sine excitation signals such as step signals, multi-pulse signals, white noise signals, etc. Onda et al. adopted the timing potential method of current step signal to measure EIS, and used Laplace transform to replace Fourier transform in data processing.<sup>6</sup> To prevent the impact of battery state of charge (SOC) variations on the EIS test results due to step signals during continuous charging and discharging, Itagaki et al. employed alternating positive and negative step signals for conducting EIS tests on the battery, thus ensuring stability of the battery SOC.<sup>7</sup> The aforementioned offline EIS test has limited practicality. To address this issue, Howey et al. implemented online measurement of EIS using the excitation signal generated by electric vehicle motor load, and assessed it with white noise excitation signal.<sup>8</sup> Meanwhile, Abareshi proposed a multi-purpose controllable EIS device based on the widely used synchronous buck converter for online and offline battery monitoring and testing during charging and discharging.<sup>9</sup> Based on the aforementioned method, considering that lithium-ion batteries typically need to be used in conjunction with power conversion circuits, we discovered that the square wave signal characteristic during the switching process is a crucial requirement for embedding the EIS test system in the power conversion circuit. Therefore, this paper proposes a fast EIS measurement method for lithium-ion batteries based on the large square wave excitation signal and designs an EIS testing device, which significantly enhances the practicality and flexibility of EIS online testing. To verify the effectiveness of the EIS test method presented in this paper, we propose an optimized equivalent circuit model (OECM) based on the observed data patterns and the lithium-ion battery electrochemical model, to perform

<sup>1</sup>Hubei University of Technology, Hubei Key Laboratory for High-efficiency Utilization of Solar Energy and Operation Control of Energy Storage System, Wuhan 430068, Hubei Province, China

<sup>2</sup>These authors contributed equally

<sup>3</sup>Lead contact

\*Correspondence:  
[jjiang@hbut.edu.cn](mailto:jjiang@hbut.edu.cn)

<https://doi.org/10.1016/j.isci.2023.106463>



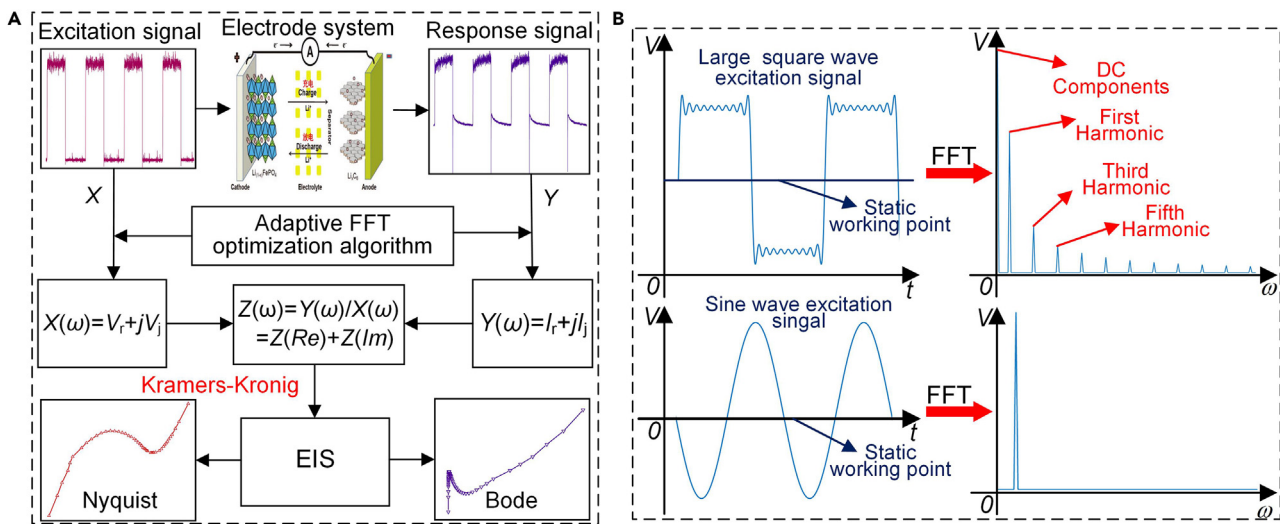


**Figure 1. EIS measurement and the comparison of the square wave signal and the sine signal after FFT**

(A) Improved EIS testing method and processing based on adaptive FFT algorithm.

(B) Differences between FFT processing of large signal square wave excitation and sine wave excitation.

recognition on the original data obtained from the EIS measurement. Meanwhile, to emphasize the superiority of OECM in fitting data, the goodness-of-fit ( $R^2$ ) under the second-order aging model is compared between OECM and the conventional equivalent circuit model (CECM).<sup>10,11</sup> Finally, it is concluded that using the  $R_{SC}$  fitted by OECM as a representation parameter of battery health state can achieve a relatively accurate estimation of battery state of health (SOH).

This paper starts by analyzing the principle of EIS measurement of the square wave excitation signal, exploring its EIS testing characteristics and constraints. Then, to implement the EIS testing conditions for the square wave excitation signal, a square wave excitation device with a response speed of microseconds was developed, and a method of controlling current and limiting voltage was used to achieve safe and reliable measurements. Finally, the proposed method and experimental data were used to estimate SOH of lithium-ion batteries.

### EIS measurement principle based on square wave excitation

#### Principle of conventional EIS measurement

Conventional EIS testing involves applying a single-frequency sine voltage signal to a battery, and collecting the corresponding current response signal at that frequency. The impedance information at that frequency can then be obtained by dividing the two signals.<sup>12,13</sup> The impedance information is in the form of a complex number, and it should be noted that a conventional EIS test only corresponds to one impedance information for one frequency. To ensure the accuracy of experimental data, multiple cycles of scanning are often performed during actual tests, and the data are processed using the Fourier algorithm.<sup>14–17</sup> The EIS testing method based on the adaptive FFT optimization algorithm is shown in (Figure 1A).

The conventional EIS testing method has high accuracy and simple data processing, but it needs to be done offline, and the excitation signal will last for a long time when conducting low-frequency impedance test.

#### Analysis of square wave EIS measurement principle

According to the definition of Fourier series, for any periodic signal  $f(t)$  in the time domain, it can be decomposed into the sum of trigonometric functions at a series of frequencies, while using Euler's formula can be further expanded into the complex form:

$$\begin{cases} f(t) = a_0 + \sum_{n=0}^{\infty} (a_n \cos n\omega t + b_n \sin n\omega t) \\ f(t) = C_0 + \sum_{n=1}^{\infty} (c_n e^{j\omega nt} + c_{-n} e^{-j\omega nt}) = \sum_{n=-\infty}^{\infty} c_n e^{-j\omega nt} \\ c_n = \frac{a_n \pm j b_n}{2} = \frac{1}{T} \int_0^T f(t) e^{-j\omega nt} dt \end{cases} \quad (\text{Equation 1})$$

When  $V(t)$  and  $I(t)$  are respectively the excitation signal and response signal in the time domain, they can be transformed into the frequency domain through [Equation 1](#), as follows:

$$\begin{cases} V(\omega) = \frac{1}{T} \int_0^T V(t) \cos \omega t dt - \frac{j}{T} \int_0^T V(t) \sin \omega t dt \\ I(\omega) = \frac{1}{T} \int_0^T I(t) \cos \omega t dt - \frac{j}{T} \int_0^T I(t) \sin \omega t dt \end{cases} \quad (\text{Equation 2})$$

Dividing  $V(\omega)$  by  $I(\omega)$  yields the impedance  $Z(\omega)$  at the corresponding frequency. The reason for focusing on a square wave excitation signal in this paper is 2-fold: on the one hand, it aligns with the square wave signal characteristic of the EIS measurement system embedded in the power conversion circuit; on the other hand, the square wave signal can be expanded through the Fourier series to obtain the sum of odd harmonic components of the sine signal,<sup>[18–20](#)</sup> meaning that a single-frequency square wave signal can contain multiple frequency information. The Fourier series expression of a square wave signal is:

$$\begin{cases} V(t) = \frac{V_s}{2} + \frac{2V_s}{\pi} \left( \sin \omega t + \frac{1}{3} \sin 3\omega t + \frac{1}{5} \sin 5\omega t + \dots + \frac{1}{n} \sin n\omega t \right) \\ \omega = \frac{2\pi}{T} \end{cases} \quad (\text{Equation 3})$$

where,  $V_s$  is the amplitude of square wave,  $T$  is the period, and  $n$  is an odd number. When  $\omega = 0$ , the DC components can be obtained:

$$V(t) = \frac{V_s}{2} \rightarrow F(\omega) = \int_0^T V(t) e^{-j\omega t} dt \quad (\text{Equation 4})$$

The comparison of the large square wave excitation signal and the sine excitation signal after FFT is shown in ([Figure 1B](#)). It can be seen from the [Figure 1B](#) that the large square wave excitation signal can be decomposed into a DC component and multiple decreasing odd harmonic components, and the analysis process of each harmonic component is similar to that of a sine wave. Conventional EIS testing involves applying a small sine excitation signal near a static working point, and we have observed that large square wave excitation signal carries out impedance testing equivalent to multiple sine EIS tests with the offset of the static working point.

It can be seen that the large square wave excitation signal has some advantages when conducting EIS testing: (a) During single-frequency sweeping testing, the square wave excitation can be seen as the superposition of multiple sine excitation signals, thus achieving a fast testing effect; (b) When performing EIS tests using the large signal, the static working point will experience a shift, thus allowing for better emulation of impedance data during charging and discharging processes of lithium-ion batteries.

It should be noted that square wave excitation may be a nonlinear process, but conventional EIS measurement is a linear process by applying small signal disturbances to the electrode system without changing the working state of the original system.<sup>[21](#)</sup> Therefore, in the second section of this paper, the constraint conditions of square wave are analyzed to meet the linearization requirements of EIS test.

### Analysis of large excitation signal characteristics and square wave excitation constraints

#### Principle analysis of large signal excitation characteristics

This paper designs an excitation power supply test device that can generate large excitation signal based on the power MOS transistor. Large excitation signal is a nonlinear transformation process, which will essentially change the original static working point. In control theory, large excitation signal can be used to judge the working state.<sup>[22](#)</sup> Next, the operating state of the MOS transistor is taken as an example to

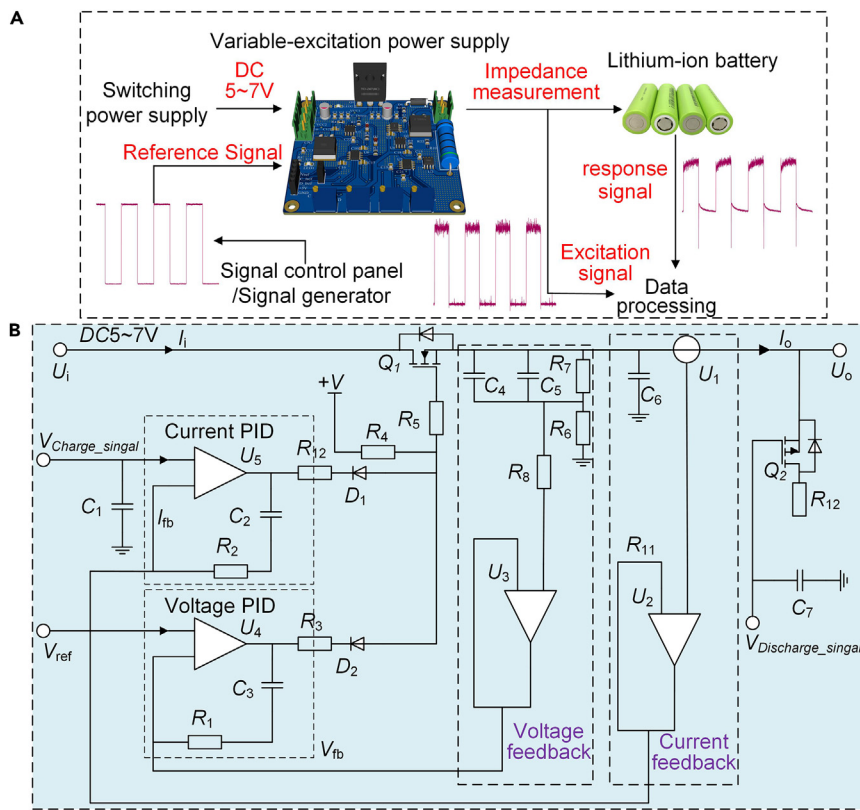


**Figure 2. EIS hardware test system**

(A) EIS hardware test system structure diagram.

(B) Simplified topology diagram of variable-excitation power supply.

analyze its large excitation signal characteristics. The architecture of the experimental system (Figure 2A) will be described in detail in the following section of the manuscript.

The MOS transistor in the excitation power supply needs to switch between cutoff and linear working range in order to output square wave excitation, which is a large signal nonlinear switching process. According to the principle of piecewise differentiation, the large signal model of MOS transistor can be subdivided into each switching process to achieve linear analysis. The large excitation signal model formula of MOS transistor linear region is:

$$I_{DS} = \frac{1}{2}u_n C_{ox} \frac{W}{L} [2(VGS - VT) - V_{DS}^2] \quad (\text{Equation 5})$$

where,  $W$  is the conductive width,  $C_{ox}$  is the capacitance per unit area, and  $V_T$  is the oxide layer voltage. The following is the derivation of the large signal model in the linear region through the leakage inductance current  $I_d$ :

$$\begin{cases} I_d = v \times Q_d \\ v(x) = \mu_n \frac{dV(x)}{dx} \\ Q_d(x) = WC_{ox}(V_{GS} - V(x) - VT) \end{cases} \quad (\text{Equation 6})$$

$v$  represents the velocity of charge, and  $Q_d$  represents the charge surface density. Furthermore, it can be derived that:

$$I_d = WC_{ox}(V_{GS} - V(x) - VT)\mu_n \frac{dV(x)}{dx} \quad (\text{Equation 7})$$

From the above derivation, it can be seen that when  $V_{GS}$  is determined, IDS is a quadratic function of  $V_{DS}$  with downward-opening curve and the maximum value is  $V_{DS} = V_{GS} - V_T$ . Also, it is possible to use large signals for determining the bias point and it can still be considered as linear analysis in the new working state. However, the size of  $V_{GS}$  must be reasonably controlled as a precondition. Otherwise, the changing process cannot be treated as linear.<sup>23</sup>

Back to battery itself, applying a square wave excitation of a certain amplitude to the battery will produce a corresponding response signal, which is a nonlinear transformation process that changes the original bias point or working state of the battery.<sup>24</sup> Through reasonable control of the amplitude, linear analysis can still be used in this nonlinear change process.

### Analysis of square wave excitation constraint conditions

For the linear condition, the amplitude of square wave excitation signal can be controlled to meet the linear analysis requirements. Two points should be paid special attention to when conducting square wave excitation EIS measurement for lithium batteries: (a) The amplitude depends on the resistance of the tested system; (b) Measurement may cause potential fluctuation, especially under low-frequency test.<sup>25,26</sup> The electrochemical model and equivalent model of lithium-ion battery is shown in (Figure 5A).

The electrochemical impedance formula of lithium-ion battery is:

$$Z = \Delta E / \Delta i \quad (\text{Equation 8})$$

where,  $\Delta i$  is the total current,  $\Delta E$  is the electrode potential, and the total current  $\Delta i$  is related to the species concentration  $\Delta c_i$  and the electrode potential  $\Delta E$ .<sup>27</sup> It can be expressed as:

$$\Delta i = \sum \left( \frac{\partial i}{\partial c_i} \right) \Delta c_i + \left( \frac{\partial i}{\partial E} \right) \Delta E + Oi^n \quad (\text{Equation 9})$$

where,  $Oi^n$  is a high-order term. Hence, neglecting the higher order terms and solving for Z:

$$Z = 1 / \frac{\partial i}{\partial E} \left[ 1 - \sum \left( \frac{\partial i}{\partial c_i} \right) \frac{\Delta c_i}{\Delta i} \right] \quad (\text{Equation 10})$$

Now, the first term is charge transfer impedance ( $R_{ct} = \partial E / \partial i$ ) and the second term relates to the influence of electrolyte and electrode diffusion effect. For details, please refer to the research of Claudio Brivio et al.<sup>28</sup> The total current of charge transfer reaction on the battery electrode is related to  $\eta_s$  overpotential. According to the Butler-Volmer equation, the following equation can be obtained:

$$\begin{cases} i = i_0 (e^{\alpha_a F \eta_s / RT} - e^{-\alpha_c F \eta_s / RT}) \\ i_0 = nFk_0 (c_O - c_R) \end{cases} \quad (\text{Equation 11})$$

where,  $i_0$  is the exchange current density;  $\alpha_a$  and  $\alpha_c$  are anodic and cathodic transfer coefficients, respectively;  $F$  is Faraday's constant;  $R$  is the gas constant;  $T$  is the absolute temperature, where the exchange current  $i_0$  depends on the concentration of oxidation state ( $c_O$ ) and reduction state ( $c_R$ ) in the charge transfer reaction.<sup>26</sup>

The Equation 11 can be expanded by Taylor series to obtain:

$$i = i_0 \left\{ \begin{array}{l} (\alpha_a + \alpha_c) \frac{F \eta_s}{RT} + \frac{(\alpha_a^2 - \alpha_c^2)}{2} \left( \frac{F \eta_s}{RT} \right)^2 \\ + \frac{(\alpha_a^3 - \alpha_c^3)}{6} \left( \frac{F \eta_s}{RT} \right)^3 + O\eta_s^4 \dots \dots \\ + \frac{(\alpha_a^n - \alpha_c^n)}{n!} \left( \frac{F \eta_s}{RT} \right)^n \dots \dots \end{array} \right\} \quad (\text{Equation 12})$$

where, typical parameter values are:  $\alpha_a = \alpha_c = 0.5$ ;  $T = 298K$ . To ensure the expression presents linear transformation, it is necessary to limit the current to be a direct current or the change less than 1%.<sup>25,26</sup> Therefore, according to the Ohm's law, the most commonly used voltage response range of lithium-ion battery is about 5–50 mV.<sup>29</sup>

In summary, the following experimental tests in this paper will control the voltage response in a reasonable range by adjusting the amplitude of the excitation current, to achieve the linear analysis condition, and further measure the EIS of lithium batteries under the large square wave excitation signal.

### System hardware design and implementation

#### System structure overview

We designed a fast EIS measurement system for lithium-ion batteries based on the large square wave excitation signal. The experimental system architecture is shown in (Figure 2A).

The working principle of the system is: the common 220 V/50 Hz power supply (in China) is converted into 5–7 V DC through power conversion to supply the excitation power module. The excitation power module selects the voltage limit value according to load type (for example, if the load is lithium-ion battery, and the voltage limit value can be selected as 4.2 V). The variable-excitation power module applies the excitation signal to electrode system based on reference signal from signal control board (or signal generator). Collect and process the excitation signal and response signal of the tested lithium-ion battery, and obtain the EIS diagram.

#### Design of variable-excitation power supply

In order to realize microsecond fast excitation response and control the voltage to prevent potential safety hazards, this paper specially designs a time-varying excitation power supply. The circuit uses a double closed-loop structure, with voltage and current as feedback control signals. The simplified topology structure of the variable-excitation power supply is shown in (Figure 2B).

In the voltage feedback circuit,  $R_6$  and  $R_7$  are high-precision voltage divider acquisition resistors,  $U_3$  push-pull output  $V_{fb}$ ,  $U_4$  is comparator, and according to the following requirements:  $V_{ref} = V_{fb} = \frac{1}{2} \cdot U_o$ . When the current feedback circuit works, the Hall current sensor  $U_1$  is firstly used to collect the excitation current, and the current feedback signal  $I_{fb}$  is obtained through the  $U_2$  push-pull output.  $U_5$  is a comparator, which is combined with the peripheral circuit to form PID regulation to quickly track the reference current. The amplitude of the output excitation current signal can be controlled not to exceed the limit by adjusting the input reference signal, thus meeting the EIS test requirements.

The resistor  $R_4$  and the diode  $D_1$  and  $D_2$  conduct “or logic” to control the gate of the MOSFET, so as to achieve the double closed-loop following control effect of voltage limiting and current controlling. The overall structure of the circuit control is simple and effective, the response speed is fast, and the experimental process is safe and reliable. The control principle of negative excitation is the same as described previously, just change the control switch from  $Q_1$  to  $Q_2$ .

### EIS test experiment

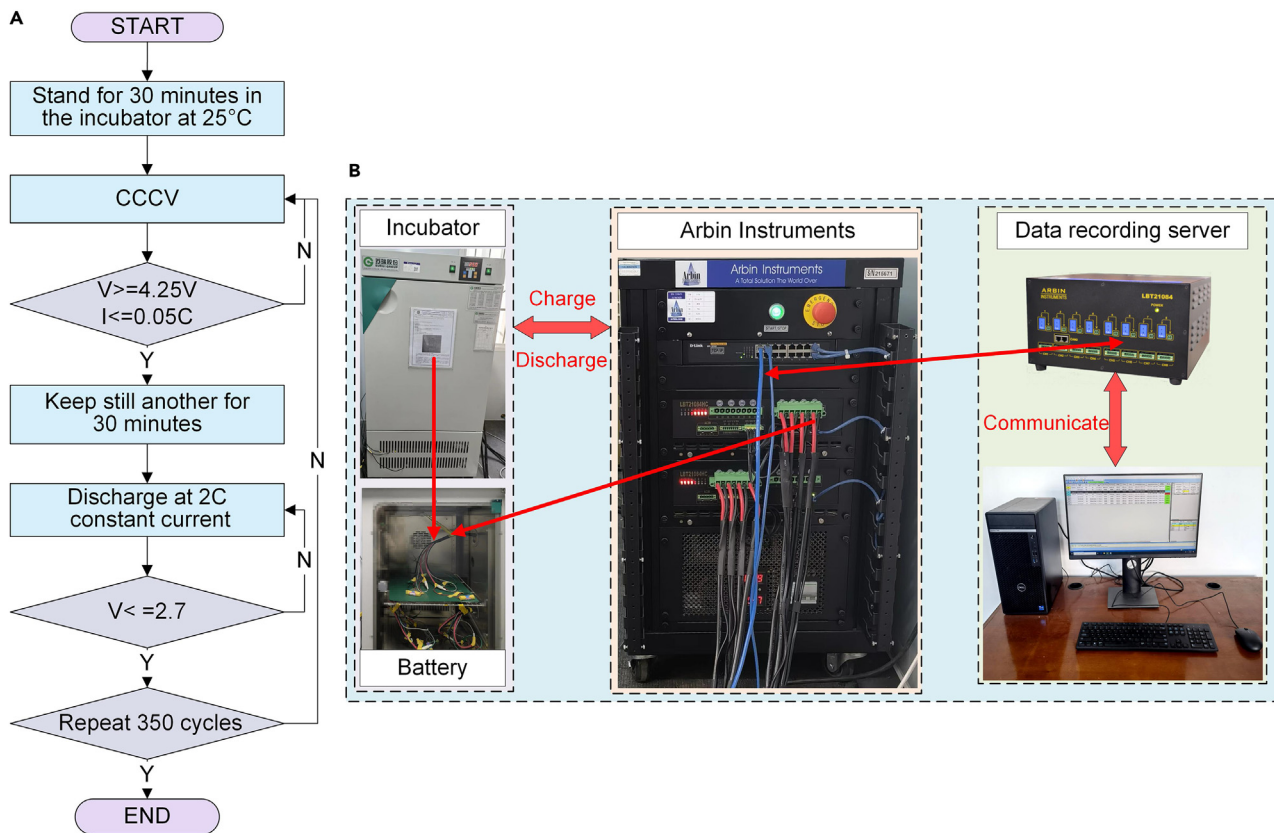
#### Test pretreatment

For subsequent EIS testing under different cycles, lithium batteries will be placed in an incubator for cyclic aging experiment. The flow chart of the above cyclic aging test (Figure 3A), and the diagram of lithium-ion battery cyclic aging are shown in (Figure 3B).

#### EIS test under the large square wave excitation signal

The actual EIS test experiment diagram is shown in (Figure 4A). To improve the controllability of the experimental test, the test process is carried out in a 25°C incubator. The comparison of the reference signal, excitation signal, and response signal at different amplitudes and frequencies is shown in (Figures 4B–4D). Figure 4B shows the reference signals, in which the square wave reference signals are 100 Hz/2–2.61 V and 150 Hz/2–2.57 V, respectively. The main difference lies in the frequency and amplitude. Figure 4C is the actual excitation signal generated according to the reference signal, and Figure 4D is the response signal of the battery. In the actual test, the amplitude and frequency of the excitation signal can be adjusted flexibly, so that more comprehensive analysis data can be obtained.

In data optimization, it is easier to handle the optimization of high-frequency and mid-frequency components, while the interference from low-frequency and mid-frequency components can increase the difficulty of data processing. Therefore, the algorithm proposed by Wojcik et al. was referred to in the data

**Figure 3. Lithium-ion battery aging cycle experiment**

(A) Flow chart of lithium-ion battery aging cycle experiment.  
(B) Experimental diagram of lithium-ion battery cyclic aging.

optimization process.<sup>25</sup> The experiment is conducted impedance test is single-frequency excitation, so the test impedance data at each frequency is not affected, so the data that do not meet the Kramers-Kronig relationship in the data processing process can be removed directly to ensure the accuracy of the test data.<sup>30,31</sup> A smoothing algorithm was applied in the subsequent data processing to clarify the trend of curve variations.

The specific operation process of the fast EIS measurement method will be shown next (Figure 4E). Firstly, the actually measured excitation current signal ( $X$ ) and the response voltage signal ( $Y$ ) are processed by the adaptive FFT optimization algorithm; then the obtained data  $X(\omega)$  and  $Y(\omega)$  in the frequency domain are used for impedance calculation, and it should be noted that to guarantee the accuracy of the impedance data, only the first three data with larger amplitude in the frequency domain are selected for impedance calculation; finally, the Kramers-Kronig theorem is used to further optimize the impedance data, to obtain the Nyquist plot of the impedance data.

### SOH estimation using correspondence between EIS and ECM

#### Optimization model for ECM

The EIS equivalent models of lithium batteries can be divided into two categories: on the one hand, the internal parameters and partial differential equations of lithium-ion batteries are used for modeling to simulate the actual structure state and reaction process of batteries; on the other hand, the equivalent circuit model (ECM) uses electrical components or electrochemical components to form a circuit, making the electrochemical impedance characteristics of the circuit the same as the impedance characteristics of the electrode system, so as to simulate the internal state of the battery.<sup>18,32,33</sup>

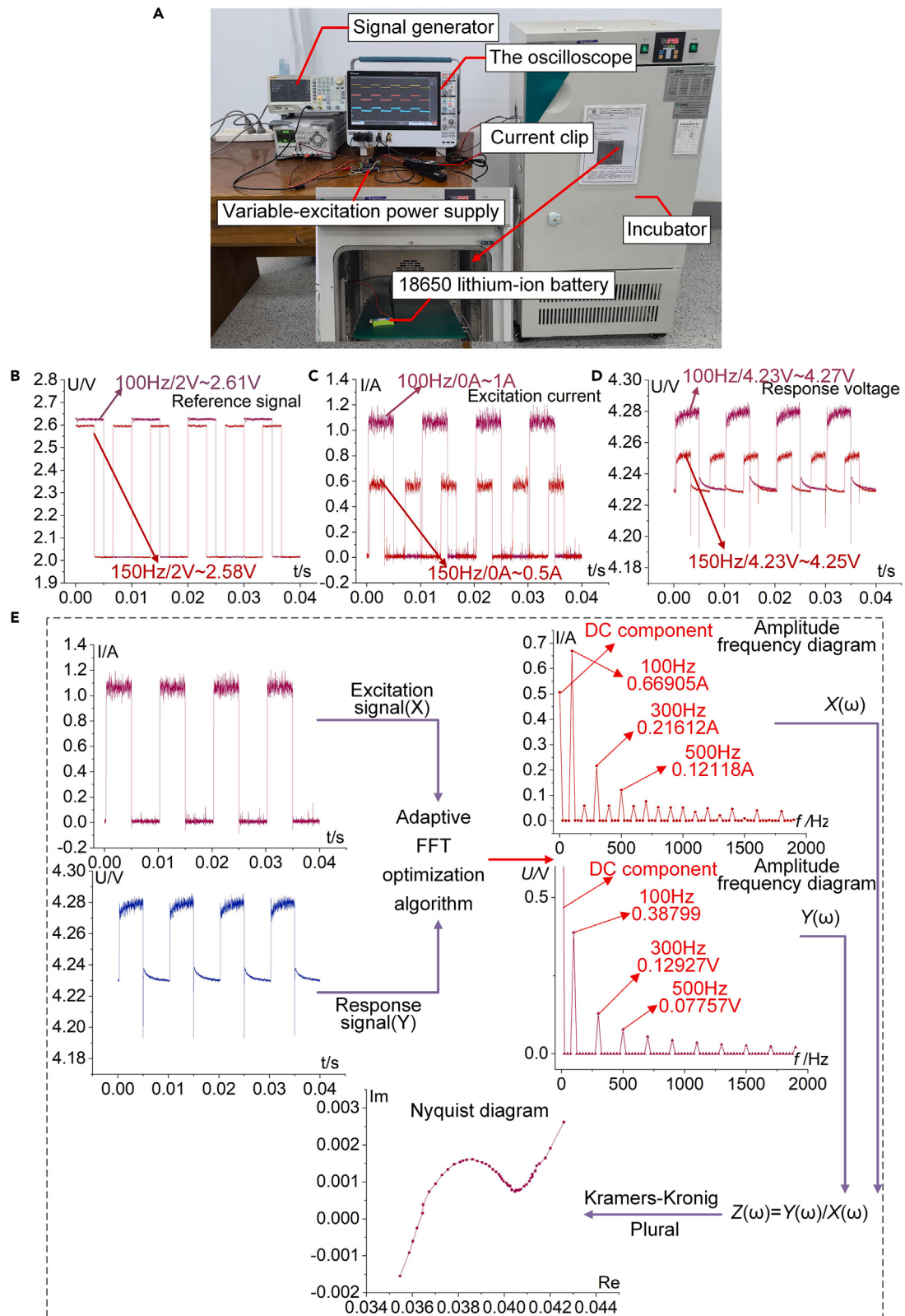


**Figure 4. EIS testing and data processing**

- (A) EIS actual test experiment diagram.
- (B) Reference signals at different frequencies and amplitudes.
- (C) Excitation signals at different frequencies and amplitudes.
- (D) Response signals at different frequencies and amplitudes.
- (E) Operation process diagram of fast EIS test method.

The fractional order equivalent model mainly includes: high-frequency inductance ( $L$ ), ohmic resistance ( $R_0$ ), constant phase element (CPE); SEI membrane impedance  $R_{SEI}$  and charge transfer  $R_{CT}$  are different processes of battery aging; low frequencies are represented by Warburg impedance ( $Z_W$ ) or CPE. The ECM approximates the EIS curve by combining the previous elements.<sup>33,34</sup> The fractional order equivalent model is composed of  $R_{SEI}$  and  $R_{CT}$  in the half-circle part, and there may be multiple half-circle cases in the actual EIS test, and such a model can be called the CECM. This paper uses the structural model of (Figure 5A) combined with the actual test data characteristics to propose an OECM for parameter fitting (Figure 5B).

The basic formula of the model is:

$$Z_{ECM} = Z_L + R_0 + Z_{R/CPE} + Z_W \quad (\text{Equation 13})$$

where,  $Z_L = j\omega L$ ,  $R_0$  is ohmic resistance, and  $Z_W$  is the Warburg impedance,<sup>35</sup> its frequency domain expression is:

$$Z_W(s) = \frac{1}{Qs^\alpha} \quad (\text{Equation 14})$$

$Q$  is the equivalent capacitance, and the value of  $\alpha$  ranges from 0 to 1. When  $\alpha = 0$ ,  $Q$  can be regarded as a resistive element, while when  $\alpha = 1$ ,  $Q$  is a capacitive element. Further expansion leads to:

$$\begin{cases} Z_W(j\omega) = \frac{1}{Q(j\omega)^\alpha} \\ j^{-\alpha} = e^{-j\frac{\alpha\pi}{2}} = \cos\frac{\alpha\pi}{2} - j\sin\frac{\alpha\pi}{2} \end{cases} \quad (\text{Equation 15})$$

The parallel transfer function between  $R_{sc}$  and CPE is:

$$Z_{R/CPE}(\omega) = \frac{R_{sc}}{1 + R_{sc}Q(j\omega)^\alpha} = \frac{R_{sc} + R_{sc}^2Q^2\omega^\alpha \cos\frac{\alpha\pi}{2} - jR_{sc}^2Q\omega^\alpha \sin\frac{\alpha\pi}{2}}{1 + R_{sc}^2Q^2\omega^{2\alpha} + 2R_{sc}Q\omega^\alpha \cos\frac{\alpha\pi}{2}} \quad (\text{Equation 16})$$

The real part and imaginary part are:

$$\begin{cases} Z_{Re} = \frac{R_{sc} + R_{sc}^2Q^2\omega^\alpha \cos\frac{\alpha\pi}{2}}{1 + R_{sc}^2Q^2\omega^{2\alpha} + 2R_{sc}Q\omega^\alpha \cos\frac{\alpha\pi}{2}} \\ Z_{Im} = \frac{-jR_{sc}^2Q\omega^\alpha \sin\frac{\alpha\pi}{2}}{1 + R_{sc}^2Q^2\omega^{2\alpha} + 2R_{sc}Q\omega^\alpha \cos\frac{\alpha\pi}{2}} \end{cases} \quad (\text{Equation 17})$$

By observing  $Z_{Re}$  and  $Z_{Im}$ , we can find that:

$$\left( Z_{Re}(\omega) - \frac{R_{sc}}{2} \right)^2 + \left( Z_{Im}(\omega) - \frac{-R_{sc} \cot\left(\frac{\alpha\pi}{2}\right)}{2} \right)^2 = \frac{R_{sc}^2}{\left(2 \sin\left(\frac{\alpha\pi}{2}\right)\right)^2} \quad (\text{Equation 18})$$

From the above Equation 18, it can be found that Re and Im meet the requirements of taking  $\left(\frac{R_{sc}}{2}, \frac{-R_{sc} \cot\left(\frac{\alpha\pi}{2}\right)}{2}\right)$  as the center of the circle, and the radius is  $\frac{R_{sc}}{2 \sin\left(\frac{\alpha\pi}{2}\right)}$  circles.

### Parameter fitting

The SOH estimation process is as follows: according to the OECM proposed above, the parameter fitting is combined with Zview software to obtain the original data, and finally using the fitted original data to estimate the SOH. After each group of data is tested, it is processed into Figures 6A and 6B. Figure 6A is the EIS

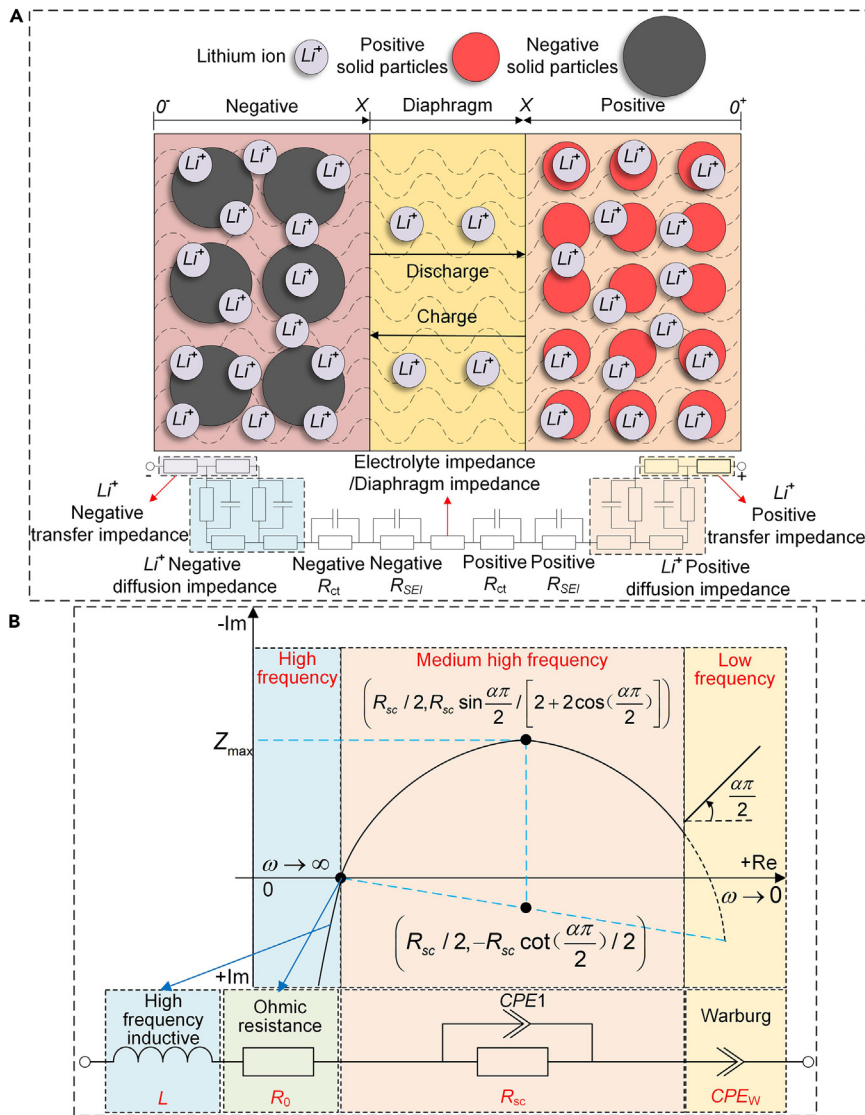


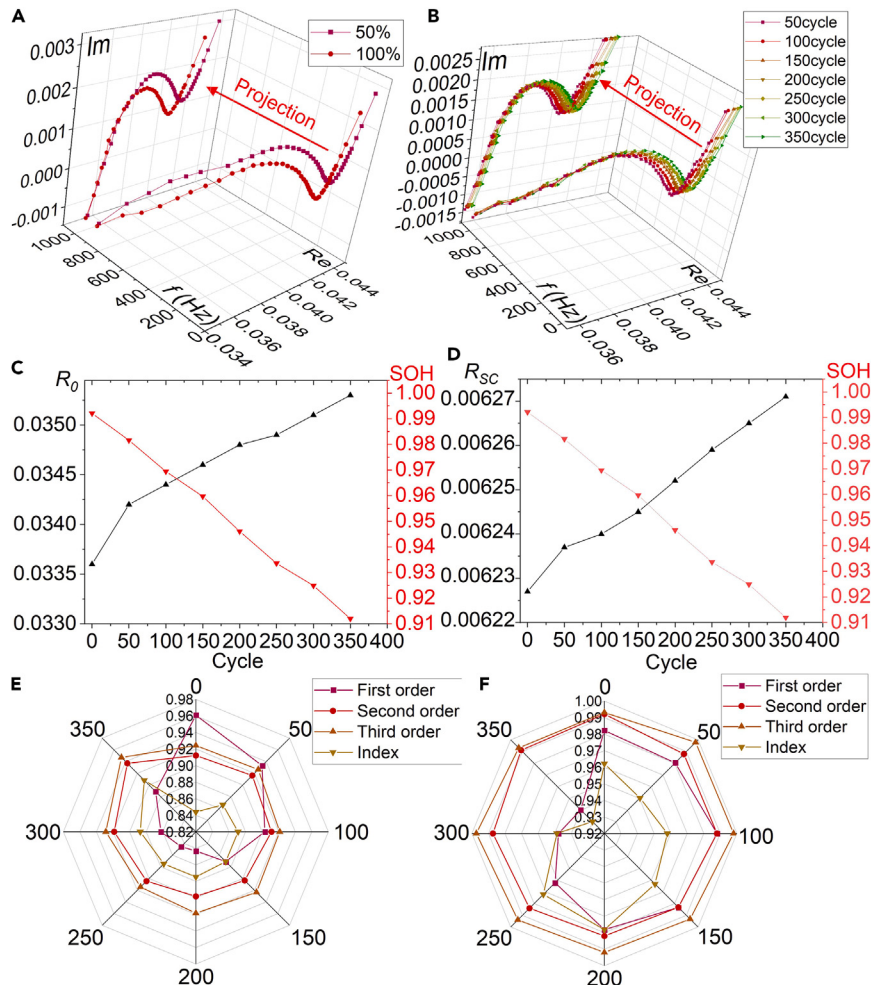
**Figure 5. Lithium-ion battery model**

(A) Schematic diagram of electrochemical model and equivalent model of lithium-ion battery.  
(B) Optimization model for ECM.

diagram of different SOC after aging for 350 times, and Figure 6B is the EIS diagram of different aging times under 100% SOC. It can be seen that the EIS diagram tested by this device has a good change regularity. Under different SOC, the EIS has little change in the high- and middle-frequency bands, and the main change and difference are in the middle- and low-frequency bands; the EIS maps with different cycles will shift to the right as a whole, compared with large shifts in the medium and low frequency bands.

After every 50 cycles, the discharge capacity of the battery will be tested by using the Arbin Instruments, and the fitting original data (Table 1). The calculation formula for SOH of lithium-ion battery is the ratio of the current maximum discharge capacity  $C_{now}$  to the rated capacity  $C_{max}$ :

$$SOH = \frac{C_{now}}{C_{max}} \cdot 100\% \quad (\text{Equation 19})$$

**Figure 6. EIS measured data and fitting data**

- (A) Impedance diagram of different SOC under 350 aging times.
- (B) Impedance diagram of different aging times under 100% SOC.
- (C) Fitting the trend chart of parameter  $R_0$  and SOH under different cycles based on OECM/100% SOC.
- (D) Fitting the trend chart of parameter  $R_{SC}$  and SOH under different cycles based on OECM/100% SOC.
- (E) Fitting data  $R_0$  of different empirical models at 100% SOC/different cycle times.
- (F) Fitting data  $R_{SC}$  of different empirical models at 100% SOC/different cycle times.

### SOH estimation

It can be seen from the above fitting parameters that, with the increase of the number of cycles and the decrease of SOH, the resistance values of  $R_0$  and  $R_{SC}$  have a significant upward trend, which reflects the relationship between impedance and SOH to a certain extent, so  $R_0$  and  $R_{SC}$  can be used as the state indicators of aging. Based on OECM/100% SOC, the fitting parameters  $R_0$ ,  $R_{SC}$ , and SOH change trends under different cycles (Figures 6C and 6D). Next, compare the goodness-of-fit of  $R_0$ ,  $R_{SC}$  pairs, and screen out more accurate characterization parameters for SOH calculation.

The empirical model of lifetime degradation is established according to the previously described fitting parameters, while the commonly used empirical models of aging are polynomial model and exponential model,<sup>36,37</sup> and the basic formula is:

$$\begin{cases} y = b + ax + cx^2 + \dots \\ y = ae^{bx} \end{cases} \quad (\text{Equation 20})$$

**Table 1.** Fitting parameters of different cycles at 100% SOC

SOH real value	Cycle	L	R <sub>0</sub> (ohm)	T <sub>CPE1</sub>	P <sub>CPE1</sub>	R <sub>Sc</sub> (ohm)	T <sub>CPEw</sub>	P <sub>CPEw</sub>
99.21%	0	4.451E-7	0.0336	0.7981	0.7143	0.006227	323.1	0.5516
98.16%	50	4.460E-7	0.0342	0.7921	0.7248	0.006237	326.9	0.5446
96.94%	100	4.384E-7	0.0344	0.7481	0.7376	0.006240	325.7	0.5525
95.97%	150	4.368E-7	0.0346	0.6851	0.7544	0.006245	320.2	0.5383
94.61%	200	4.217E-7	0.0348	0.6066	0.7815	0.006252	311.9	0.5254
93.36%	250	4.474E-7	0.0349	0.6400	0.7686	0.006259	319.6	0.5409
92.49%	300	4.399E-7	0.0351	0.6290	0.7664	0.006265	313.3	0.5240
91.20%	350	4.432E-7	0.0353	0.6135	0.7796	0.006271	313.4	0.5345

Y is the characterization parameter corresponding to aging, and x is the number of cycles. At the same time, the goodness-of-fit ( $R^2 = 1 - R_{SS}/T_{SS}$ ) value of parameters was introduced to evaluate the good and bad degree of the fitting of the basic formula of different models.<sup>38</sup> The value of goodness-of-fit ( $R^2$ ) is between 0 and 1, and the closer it is to 1, the better the fitting effect will be. The calculation formula is:

$$\left\{ \begin{array}{l} R_{SS} = \sum_{i=1}^n (y_i - y'_i)^2 \& T_{SS} = \sum_{i=1}^n (y_i - y'')^2 \\ R^2 = 1 - \frac{\sum_{i=1}^n (y_i - y'_i)^2}{\sum_{i=1}^n (y_i - y'')^2} \end{array} \right. \quad (\text{Equation 21})$$

In the above equation,  $y_i$  represents the i-th original data,  $y'_i$  is the calculated value of aging model,  $y''$  is the average value of the original data, and n is the number of fitted data points. By using [Equation 21](#),  $R_0$  and  $R_{Sc}$  are compared in terms of fitting quality and the parameters that represent the best fit result are selected. The  $R^2$  of different aging empirical models at 100% SOC for different cycles is shown in ([Figures 6E](#) and [6F](#)).

To highlight the superiority of OECM in fitting the original parameters, we will compare it with CECM in terms of fitting the original parameters. After the actual operation, it can be found that the same set of actual test data has a large fitting error and fitting failure in the process of fitting the original parameters using CECM, while comparing the data, it is found that only  $R_0$  can be used as a characterization parameter for battery aging (The  $R_0$  goodness-of-fit value of CECM under the second-order aging model is 0.9448, which is lower than the  $R_0$  goodness-of-fit value of OECM under the second-order aging model of 0.9525). Other scholars have done the same study, for example: Chang Chun et al.<sup>43</sup> proposed an equivalent circuit model (MLECM) based on fusing SEI film resistance and charge transfer resistance in the low- and medium-frequency domains for fitting the original parameters and comparing the goodness-of-fit values of the second-order aging models for different battery types. The previously described article<sup>39</sup> is similar to the OECM proposed in this paper, so as to further verify the superiority of OECM in estimating

**Table 2.** Goodness-of-fit values of OECM and CECM under the second-order aging model

Battery	OECM/MLECM	CECM	Optimal Superiority Parameter/Model
	R <sub>Sc</sub> (ohm)	R <sub>CT</sub> (ohm)	
INR18650-26E	0.9869	None	R <sub>Sc</sub> /OECM
25C05# <sup>[43]</sup>	0.9657	0.8908	R <sub>Sc</sub> /MLECM
35C02# <sup>[43]</sup>	0.9909	0.9814	R <sub>Sc</sub> /MLECM
45C02# <sup>[43]</sup>	0.9974	0.9565	R <sub>Sc</sub> /MLECM
NCA1# <sup>[43]</sup>	0.9644	0.9734	R <sub>CT</sub> /CECM
NCA2# <sup>[43]</sup>	0.9871	0.9664	R <sub>Sc</sub> /MLECM

**Table 3. Comparison of the real true and estimated values of SOH and errors for the second-order model**

Cycle	SOH true value	SOH estimation	Absolute error
0	99.21%	97.134%	2.08%
50	98.16%	95.97%	2.19%
100	96.94%	94.804%	2.14%
150	95.97%	95.193%	0.78%
200	94.61%	92.468%	2.14%
250	93.36%	91.493%	1.87%
300	92.49%	90.321%	2.17%
350	91.20%	88.559%	2.64%

SOH. The goodness-of-fit values of OECM/MLECM and CECM under the second-order aging model are shown in (Table 2).

According to the previous analysis on the goodness-of-fit ( $R^2$ ) of OECM/MLECM and CECM under the second-order aging model, it can be seen that OECM/MLECM is superior to CECM in overall fitting. At the same time, the goodness-of-fit of  $R_0$  is lower than  $R_{SC}$  when OECM is used to fit data. In summary, the superiority of the CECM model fitting parameters is poorer than OECM, and the  $R_{SC}$  fitting values under the second-order model of OECM can be chosen for more accurate estimation of SOH. The results of SOH estimation by the  $R_{SC}$  fitting parameters under the second-order model are shown in (Table 3).

The above experimental procedure was carried out by establishing the OECM to fit the parameters, and the best-fit parameters were selected for SOH estimation by combining the  $R^2$ . Compared with the EIS equivalent model-based SOH estimation method proposed by other scholars with an error of 4.5%,<sup>40</sup> the OECM proposed in this paper can control the quasi-error of SOH estimation to 3%, which has better estimation accuracy and less computation.

### Limitations of the study

Aiming at the limitations of EIS testing by conventional electrochemical workstations and the characteristics of power electronic circuit operation, this paper proposes a fast EIS measurement method and SOH estimation application for lithium batteries based on the large square wave excitation signal, using the designed device to perform comparative EIS testing of lithium batteries at different cycle counts and SOC. By comparing OECM with CECM, the superiority of OECM fitted data for SOH estimation is derived. This article confirms the feasibility of large wave excitation signal testing EIS through both theoretical derivation and experimentation, providing new insight into EIS testing and applications. In addition, utilizing a self-designed EIS testing device, future research can continually expand to encompass new experimental subjects (such as super capacitors) and test impedance data of novel materials. For post-processing of the test data, intelligent algorithms such as neural networks can be incrementally incorporated.

### STAR★METHODS

Detailed methods are provided in the online version of this paper and include the following:

- KEY RESOURCES TABLE
- RESOURCE AVAILABILITY
  - Lead contact
  - Materials availability
  - Data and code availability
- EXPERIMENTAL MODEL AND SUBJECT DETAILS
- METHOD DETAILS
  - Battery specifications
  - Cycling experiments
  - Impedance testing experiment
  - Optimal selection of excitation signal
  - Signal acquisition and processing
- QUANTIFICATION AND STATISTICAL ANALYSIS

## ACKNOWLEDGMENTS

This work was supported by the Key Technology Research and Development Program of Hubei (Grant No. 2022BID012) and the Natural Science Foundation of Hubei Province (Grant No. 2022CFB404).

## AUTHOR CONTRIBUTIONS

Conceptualization: L.J.W. and Z.A.S. Methodology: L.J.W. and Z.A.S. Funding acquisition: L.J.W. and J.C.J. Project administration: L.J.W. and J.C.J. Supervision: L.J.W. and J.C.J. Data curation: Z.A.S. and L.J.Z. Writing – original draft: Z.A.S. Writing – review and editing: L.J.W. and Z.A.S. All authors have read and agreed to the published version of the manuscript.

## DECLARATION OF INTERESTS

The authors declare no conflict of interests.

Received: December 9, 2022

Revised: February 27, 2023

Accepted: March 17, 2023

Published: March 22, 2023

## REFERENCES

1. Eftekhari, A. (2017). LiFePO4/C nanocomposites for lithium-ion batteries. *J. Power Sources* 343, 395–411.
2. Ma, X., Chen, M., Zheng, Z., Bullen, D., Wang, J., Harrison, C., Gratz, E., Lin, Y., Yang, Z., Zhang, Y., et al. (2021). Recycled cathode materials enabled superior performance for lithium-ion batteries. *Joule* 5, 2955–2970.
3. Li, D., Wang, L., Duan, C., Li, Q., and Wang, K. (2022). Temperature prediction of lithium-ion batteries based on electrochemical impedance spectrum: a review. *Int. J. Energy Res.* 46, 10372–10388.
4. Munichandraiah, N., Scanlon, L.G., and Marsh, R.A. (1998). Surface films of lithium: an overview of electrochemical studies. *J. Power Sources* 72, 203–210.
5. Li, D., Yang, D., Li, L., Wang, L., and Wang, K. (2022). Electrochemical impedance spectroscopy based on the state of health estimation for lithium-ion batteries. *Energies* 15, 6665.
6. Onda, K., Nakayama, M., Fukuda, K., Wakahara, K., and Araki, T. (2006). Cell impedance measurement by Laplace transformation of charge or discharge current-voltage. *J. Electrochem. Soc.* 153, A1012–A1018.
7. Itagaki, M., Ueno, M., Hoshi, Y., and Shitanda, I. (2017). Simultaneous determination of electrochemical impedance of lithium-ion rechargeable batteries with measurement of charge-discharge curves by wavelet transformation. *Electrochim. Acta* 235, 384–389.
8. Howey, D.A., Mitcheson, P.D., Yufit, V., Offer, G.J., and Brandon, N.P. (2014). Online measurement of battery impedance using motor controller excitation. *IEEE Trans. Veh. Technol.* 6, 2557–2566.
9. Abareshi, M., Sadeghi, E., Hamzeh, M., Saif, M., and Alavi, S.M.M. (2022). Multi-purpose controllable electrochemical impedance spectroscopy using bidirectional DC–DC converter. *J. Energy Storage* 55, 105750.
10. Cai, L., Meng, J., Stroe, D.I., Peng, J., Luo, G., and Teodorescu, R. (2020). Multi-objective optimization of data-driven model for lithium-ion battery SOH estimation with short-term feature. *IEEE Trans. Power Electron.* 35, 11855–11864.
11. Liu, Z., Zhao, J., Wang, H., and Yang, C. (2020). A new lithium-ion battery SOH estimation method based on an indirect enhanced health indicator and support vector regression in PHMs. *Energies* 13, 830.
12. Jiang, B., Zhu, J., Wang, X., Wei, X., Shang, W., and Dai, H. (2022). A comparative study of different features extracted from electrochemical impedance spectroscopy in state of health estimation for lithium-ion batteries. *Appl. Energy* 322, 119502.
13. Guo, Y., Yang, D., Zhang, Y., Wang, L., and Wang, K. (2022). Online estimation of SOH for lithium-ion battery based on SSA-Elman neural network. *Prot. Control Mod. Power Syst.* 7, 40.
14. Waligo, A., and Barendse, P. (2016). A Comparison of the Different Broadband Impedance Measurement Techniques for Lithium-Ion Batteries (IEEE Energy Conversion Congress and Exposition), pp. 1–7.
15. FAN, W., XU, G., YU, B., et al. (2021). On-line estimation method for internal temperature of lithium-ion battery based on electrochemical impedance spectroscopy. *J. Proceedings of the CSEE* 41, 3283–3293.
16. WEI, G. (2020). Design of Rapid State Evaluation System for Lithium-Ion Battery Based on Impedance Spectroscopy (D. Harbin Institute of Technology).
17. CAO, Chu'nan, and ZHANG, J. (2016). An Introduction to Electrochemical Impedance Spectroscopy (Science Press), pp. 20–36.
18. Orazem, M.E., and Tribollet, B. (2014). *Electrochemical Impedance Spectroscopy* (Chemical Industry Press).
19. Skvarenina, T.L. (2018). *The Power Electronics Handbook* (M. CRC Press).
20. Borio, D. (2013). Square wave decomposition for fast correlation in DSSS receivers. *IEEE Trans. Aerosp. Electron. Syst.* 49, 969–981.
21. Zhang, Q., Huang, C.G., Li, H., Feng, G., and Peng, W. (2022). Electrochemical impedance spectroscopy based state-of-health estimation for lithium-ion battery considering temperature and state-of-charge effect. *IEEE Trans. Transp. Electricif.* 8, 4633–4645.
22. Fiorelli, R., Barabino, N., Silveira, F., and Peralfas, E. (2019). Normalized nonlinear semiempirical MOST model used in monolithic RF class A-to-C pas. *Circuits Syst. Signal Process.* 39, 2796–2821.
23. Sihvo, J., Roinila, T., and Stroe, D.-I. (2021). Novel fitting algorithm for parametrization of equivalent circuit model of Li-ion battery from broadband impedance measurements. *IEEE Trans. Ind. Electron.* 68, 4916–4926.
24. Streijl, R.C., Winkler, S., and Hands, D.S. (2016). Mean opinion score (MOS) revisited: methods and applications, limitations and alternatives. *Multimed. Syst.* 22, 213–227.
25. T Wojcik, P., Agarwal, P., and E Orazem, M. (1996). A method for maintaining a constant potential variation during galvanostatic regulation of electrochemical impedance measurements. *Electrochim. Acta* 41, 977–983.
26. Wojcik, P.T., and Orazem, M.E. (1998). Variable-amplitude galvanostatically modulated impedance spectroscopy as a tool for assessing reactivity at the corrosion

- potential without distorting temporal evolution of the system. *J. Corrosion.* 54, 289–298.
27. Deng, Z., Zhang, Z., Lai, Y., Liu, J., Li, J., and Liu, Y. (2013). Electrochemical impedance spectroscopy study of a lithium/sulfur battery: modeling and analysis of capacity fading. *J. Electrochem. Soc.* 160, A553–A558.
28. Brivio, C., Musolino, V., Merlo, M., and Ballif, C. (2019). A physically-based electrical model for lithium-ion cells. *IEEE Trans. Energy Convers.* 34, 594–603.
29. Ran, L., Wu, J., Wang, H., and Li, G. (2010). Prediction of State of Charge of Lithium-Ion Rechargeable Battery with Electrochemical Impedance Spectroscopy Theory (5th IEEE Conference on Industrial Electronics and Applications), pp. 684–688.
30. Giner-Sanz, J.J., Ortega, E.M., and Pérez-Herranz, V. (2016). Application of a MonteCarlo based quantitative Kramers-Kronig test for linearity assessment of EIS measurements. *Electrochim. Acta* 209, 254–268.
31. Kronig; Josa, R.D.L.J. (1926). On The Theory of dispersion of X-rays. *J.* 12, 547–557.
32. Lévesque, L. (2014). Nyquist sampling theorem: understanding the illusion of a spinning wheel captured with a video camera. *Phys. Educ.* 49, 697–705.
33. Heinrich, M., Wolff, N., Harting, N., Laue, V., Röder, F., Seitz, S., and Krewer, U. (2019). Cover feature: physico-chemical modeling of a lithium-ion battery: an ageing study with electrochemical impedance spectroscopy (batteries & supercaps 6/2019). *Batter. Supercaps* 2, 494.
34. Rahn Christopher, D., Wang, C., and Yang. (2013). *Battery Systems Engineering* (John Wiley & Sons Ltd).
35. Pauliuikaite, R., Ghica, M.E., Fatibello-Filho, O., and Brett, C.M. (2010). Electrochemical impedance studies of chitosan-modified electrodes for application in electrochemical sensors and biosensors. *Electrochim. Acta* 55, 6239–6247.
36. Guha A, Patra A, Vaisakh K. (2017). Remaining useful life estimation of lithium-ion batteries based on the internal resistance growth model. C. 2017 Indian Control Conference (ICC), Guwahati, India. IEEE. 33–38.
37. SAHA, B., GOEBEL, K., Poll, S., and Christphersen, J. (2009). Prognostics methods for battery health monitoring using a Bayesian framework. *IEEE Trans. Instrum. Meas.* 58, 291–296.
38. Xiao, H., Tao, Z., Bai, H., Wang, H., Fu, Y., Si, N., and Bai, H. (2020). State of charge effects on the parameters of electrochemical impedance spectroscopy equivalent circuit model for lithium ion batteries. *IOP Conf. Ser. Earth Environ. Sci.* 474, 052038.
39. Chang, C., Wang, S., Tao, C., Jiang, J., Jiang, Y., and Wang, L. (2022). An improvement of equivalent circuit model for state of health estimation of lithium-ion batteries based on mid-frequency and low-frequency electrochemical impedance spectroscopy. *Measurement* 202, 111795.
40. WANG, S., WU, X., et al. (2021). A method for estimating the State of Health of retired lithium batteries. *J. Mechanical Science and Technology for Aerospace Engineering* 105, 1–11.
41. Valiūnienė, A., Sabirovas, T., Petronienė, J., and Ramanavicius, A. (2020). Towards the application of fast Fourier transform - scanning electrochemical impedance microscopy (FFT-SEIM). *J. Electroanal. Chem.* 864, 114067.

## STAR★METHODS

### KEY RESOURCES TABLE

REAGENT or RESOURCE	SOURCE	IDENTIFIER
Software and algorithms		
MATLAB version 2020	Mathworks	<a href="https://www.mathworks.com/products/matlab.html">https://www.mathworks.com/products/matlab.html</a>
ZView version 2	scribner	<a href="https://www.scribner.com/">https://www.scribner.com/</a>
Keil uVision5	arm	<a href="https://www.arm.com/company/contact-us/keil-support">https://www.arm.com/company/contact-us/keil-support</a>

### RESOURCE AVAILABILITY

#### Lead contact

Further information and requests for resources and reagents should be directed to and will be fulfilled by the lead contact, Jiuchun Jiang ([jcjiang@hbut.edu.cn](mailto:jcjiang@hbut.edu.cn)).

#### Materials availability

The study did not generate new unique reagents.

#### Data and code availability

- All data needed to evaluate the conclusions in the paper are present in the paper.
- Any additional information required to reanalyze the data reported in this paper is available from the [lead contact](#) upon request.

### EXPERIMENTAL MODEL AND SUBJECT DETAILS

The model used in this paper is the electrochemical model or equivalent circuit model of the electrochemical impedance spectroscopy of a lithium-ion battery, which can use electrical components or electrochemical components to form a circuit, so that the electrochemical impedance characteristics of the circuit are the same as the impedance characteristics of the electrode system, thus simulating the internal state of the battery.

### METHOD DETAILS

#### Battery specifications

The selected battery for the experiment is an 18650 lithium-ion battery (INR18650-26E), with a full capacity of 2550mAh, rated voltage of 3.65V, charging cutoff voltage of 4.25V, discharging cutoff voltage of 2.7V, and initial internal resistance of 35 mΩ.

#### Cycling experiments

The lithium-ion battery cycling aging experiment was conducted using an Arbin instrument (LBT21084HC), purchased from Arbin Instrument Company in the United States. To ensure that other factors such as temperature do not affect the experimental process, the test battery was placed in a constant temperature box, which was purchased from China's Surui Corporation. The total number of cycles designed for the battery cycling aging experiment in this study was 350. The specific cycling process is as follows: at the beginning of each cycle, the battery was stationary for 30 min in a constant temperature box at 25°C. Subsequently, the battery was charged in CCCV mode using an Arbin instrument. First, a constant current of 1C was used for charging, and when the charging current was less than 0.02C, it was switched to constant voltage charging until the battery reached 4.25V, at which point the charging was stopped. After charging, the battery was also kept for 30 min. Then, the battery was discharged with a current of 2C until the cutoff voltage of 2.7V was reached, completing one cycle process. During the lithium-ion battery cycling aging process, EIS was measured every 50 cycles.

### Impedance testing experiment

In this experiment, impedance tests were conducted by applying a large square wave current signal to the battery to obtain the corresponding response voltage signal. To ensure the stability of the testing environment, the experimental battery should first be placed in a constant temperature box. Then, the frequency, amplitude, and signal type of the reference signal were adjusted according to the requirements. Subsequently, the excitation signal and response signal were collected. The impedance data are also affected by the different SOC of the battery, so the SOC of the battery must be controllable during the impedance test. Multiple cycles should be included when applying the excitation signal to the battery.

### Optimal selection of excitation signal

Amplitude selection: In order to ensure the linear analysis conditions of EIS test are still met under the large excitation signal, which applied to lithium-ion battery cannot be too large. The internal resistance of lithium-ion battery is small and generally does not exceed 50 mΩ. According to the theoretical derivation in Section 2 and many practical tests, it is found that the best test effect is to control the amplitude of large excitation signal at about 1A.

Frequency selection: Because the full frequency charged chemical impedance spectrum test involves high frequency to low frequency, corresponding to different electrochemical reaction states of lithium-ion battery, and considering that the square wave excitation current signal is selected for the test experiment, so this experiment takes 0.1Hz as the lower limit and 1 kHz as the upper limit. Due to the interference in the actual test, the amplitude of the harmonic wave after FFT transformation may be equal to the amplitude of the interference signal. Therefore, the first three data points with large harmonic amplitude are selected for impedance calculation to ensure accuracy.

Initial phase selection: The initial phase has no special requirements for the selection of excitation signal. In order to ensure the uniformity of the test experiment, the initial phase is set as  $\varphi = 0$ .

### Signal acquisition and processing

Frequency changes are involved in the testing process of test data. According to Nyquist sampling theorem,<sup>41</sup> the minimum sampling frequency ( $F_s$ ) is twice the maximum frequency ( $f_{\max}$ ):  $F_s \geq f_{\max}$ .

The data acquisition depth and data length will change with the change of frequency. In order to make the FFT transformed data correspond to the actual frequency more accurately, this paper proposes an "Adaptive FFT optimization algorithm" for data processing. The specific optimization methods can be divided into three aspects: acquisition depth, small-range mean screening and threshold contrast processing.

Acquisition depth: The data acquisition depth will directly affect the amplitude and frequency after data processing. The formula for calculating the sampling frequency ( $F_s$ ) is as follows:

$$\left\{ \begin{array}{l} F_s = \frac{1}{t_{fi+1} - t_{fi}} \\ t_{fi} = \frac{\sum_a^{(N/X) \cdot i} t_a}{N/X}; a = 1 + (N/X) \cdot (i - 1) \end{array} \right.$$

In the formula,  $t_{fi}$  is discrete data point in time domain,  $i$  is the natural number (The range is 0~ $N/X$ ),  $N$  is the original data length,  $X$  is the data length to be processed, and  $N/X$  is the number of each data point; Small-range mean screening: During the test, the signal frequency is constantly changing, which makes the acquisition depth of data acquisition different, and the number of data points processed each time cannot maintain good consistency. In this paper, we use a small range mean screening to recombine the original data points, and the calculation formula is as follows:

$$\left\{ \begin{array}{l} N'_i = \frac{\sum_a^{(N/X) \cdot i} N_a}{N/X} \\ a = 1 + (N/X) \cdot (i - 1) \end{array} \right.$$

Where  $N_a$  is the original data point;  $i$  is the natural number (the range is  $0 \sim N/X$ );  $N$  is the length of the original data;  $X$  is the length of the data to be processed;  $N/X$  is the number of data points in each copy;  $N'$  is the new data point.

threshold contrast processing: This method mainly deals with two problems, On the one hand, to solve the problem that too many data points cause the amplitude and phase angle of the processed data to overlap, on the other hand, the amplitude of the data processed by the algorithm gradually decreases, which will be equal to the amplitude of the noise signal, thus affecting the screening of useful information. For this reason, the minimum harmonic amplitude required in this paper is  $A$  and  $P$ , and the data is selected by comparing with  $A$  and  $P$  (Less than  $A$  and  $P$  can be equivalent to 0).

### QUANTIFICATION AND STATISTICAL ANALYSIS

The statistical analyses in this paper were performed using MATLAB (version 2018). The data were processed by considering the data characteristics from three aspects: the sampling depth, small-scale averaging, and threshold comparison. In addition, an appropriate smoothing algorithm was applied to the data.